The cleavage of phosphodiester bonds within small RNA bulges in the presence and absence of metal ion catalysts †

Ulla Kaukinen,[a] Lukasz Bielecki,[b] Satu Mikkola,[b]* Ryszard W. Adamiak[b]* and Harri Lönnberg[a]

[a] *Department of Chemistry, University of Turku, FIN-20014, Turku, Finland*
[b] *Institute of Bioorganic Chemistry, Polish Academy of Sciences, 61-704 Poznan, Poland*

Received (in Cambridge, UK) 19th March 2001, Accepted 25th April 2001
First published as an Advance Article on the web 24th May 2001

This work studies the effect of RNA structure on the reactivity of RNA phosphodiester bonds. The aim of the study is to evaluate those structural parameters that affect reactivity to support the development of sequence-specific RNA cleaving agents. The cleavage of phosphodiester bonds within one- to five-nucleotide bulges has been studied in buffer solutions (pH 8.4), and in the presence of Zn^{2+} aqua ion (pH 6.4) or its 1,5,9-triazacyclododecane complex (pH 7.4). Molecular modelling has been applied to study the structure of the substrates. The basis of the reactivity and the catalytic potential of metal ion-based cleaving agents are discussed.

Introduction

The development of sequence-selective RNA cleaving reagents, artificial RNases, has attracted considerable attention over the last decade.[1–6] It is hoped that these cleaving agents will offer novel methods to treat viral infections, cancer, hereditary diseases or antibiotic-resistant bacterial infections. The general concept for the design of such agents is simple: an oligonucleotide recognises the target RNA sequence by hybridisation and its catalytically active function, once attached, induces a chemical modification that inactivates the target molecule. The inactivation most often is based on the action of a metal ion chelate, which enhances either the cleavage of RNA 3′,5′-phosphodiester bonds by intramolecular transesterification (Scheme 1),[1–6] or promotes the hydrolysis of the triphosphate

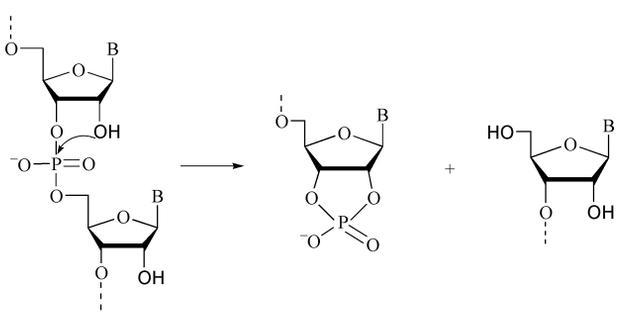

Scheme 1 The cleavage of RNA 3′,5′-phosphodiester bonds by intramolecular transesterification.

moiety in an mRNA *cap*-structure.[7] Numerous studies using simple RNA mimics have been carried out to find efficient catalysts for both the cleavage of phosphodiester bonds[1,8–11] and phosphoanhydrides.[12–14]

In the search for efficient cleaving agents, simple RNA mimetics are generally used as substrates. It is known, however, that as the structure of the substrate becomes more complicated, it starts to affect the reactivity of the phosphodiester bonds, both in the absence[15–17] and in the presence of metal ion catalysts.[18] The phosphodiester bonds within hairpin loops, for example, are less susceptible to Zn^{2+} ion-promoted cleavage than those within random-coil RNA fragments.[18] This is most probably because the hairpin structure prevents the bidentate binding of the metal ion catalyst.[19,20] The metal ion-promoted cleavage may also be accelerated by structural motifs that allow tight binding and proper positioning of several metal ion catalysts, and several examples of structures that are efficiently and site-specifically cleaved by metal ions are known.[21]

As mentioned above, the secondary structure may also affect the inherent reactivity of the phosphodiester bonds. It has been suggested that in a linear random-coil RNA molecule, the phosphodiester bonds are free to rotate and hence able to adopt the in-line conformation required for efficient cleavage.[15] Increasing rigidity of structure may retard this conformational change and hence the cleavage of phosphodiester bonds. As an example, 3′,5′-phosphodiester bonds within double-stranded RNA are clearly less reactive than those within single-stranded RNA.[17,18,22–24] It has been suggested that the presence of even a single bulged nucleotide relaxes the phosphate backbone, allowing the transition to the in-line conformation and therefore the cleavage of the RNA strand.[24]

The effect of secondary structure on the inherent reactivity may also be rate-accelerating. Phosphodiester bonds within a bulge region of ATP binding aptamer[16] or within some small hairpin loops,[17] for example, have been observed to be more reactive than those within a conformationally relaxed oligonucleotide. Besides the flexibility of the chain, a factor that is believed to play a role in this respect is the interatomic distance between the 2′-oxygen nucleophile and the phosphorus atom. A short "attack distance", less than 3.25 Å, has been suggested to increase the frequency of productive collision and therefore accelerate the reaction.[16,25] Both the flexibility and the attack distance are governed by several structural factors, such as backbone and sugar ring conformation, base stacking and intramolecular hydrogen bonding.

The present work is aimed at facilitating the development of artificial nucleases by studying the factors that affect the efficiency of the hydrolytic cleavage of phosphodiester bonds within RNA fragments having a defined secondary structure. Bulge structures studied in the present work are particularly interesting in this respect. It has been speculated[23,24,26] that if

† Electronic supplementary information (ESI) available: Graphs showing the changes in pseudorotation angle and stacking parameters undergone during the molecular dynamics simulations for compounds **4**, **6** and **13**. See http://www.rsc.org/suppdata/p2/b1/b102519h/

 DOI: 10.1039/b102519h

the cleavage is to be a *catalytic* process, it should take place *within* the double-stranded region formed upon the hybridisation of the artificial nuclease and its target RNA. Only then could an efficient turnover be expected. As phosphodiester bonds within double-stranded RNA are known to be unreactive,[17,18,22–24] the nuclease sequence should be chosen in such a manner that the target RNA, when hybridised, is forced to form a bulge structure, and that the cleavage site lies within this bulge. The results of the present study, in part, elucidate the structural requirements for the bulges that must be fulfilled for efficient action of the artificial cleaving agent.

Results

Structures of the oligonucleotides studied

Fig. 1 shows the compounds studied: dinucleoside monophosphate **1** and chimeric ribo/2′-*O*-methylribooligonucleotides **2**–**14**, mostly hairpins having a bulge at the stem. All the oligomers contain only one ribo unit, the rest of the nucleosides being 2′-*O*-methylated. Accordingly, only one of the phosphodiester bonds in each molecule may be cleaved by intramolecular transesterification. This allows accurate determination of the cleavage rate of one particular bond. 2′-*O*-Methylnucleoside units were chosen, not only in order to prevent RNA degradation, but also due to their preferred 3′-*endo*-conformation of the 2′-*O*-methylribose moiety, resembling that in natural ribonucleotide units.[27]

Compounds **1**, uridylyl-3′,5′-uridine (UpU) and **2**, a 13-mer oligouridine sequence, have been used as model compounds for a linear random-coil RNA. Uracil was chosen as a base because the stacking interactions between uracil bases are known to be of minor importance.[28] Phosphodiester bonds within structures **1** and **2** are hence free to rotate and adopt an in-line conformation during the intramolecular transesterification reaction. Compound **3** has been used as a linear reference structure to study metal-ion promoted cleavage. The base sequence of **3** is similar to that around the scissile bond in molecules **5**–**7** and **9**.

Oligonucleotides **4**–**13** form hairpins containing a bulge loop. The parent structure for these compounds is the Group I intron from *Tetrahymena thermophila*, a five-nucleotide bulge loop, the structure of which has been solved by NMR.[29] The base sequence of compound **6** is almost identical to that of the Group I intron. Only the base pair U12·A19 of the Group I intron has been replaced with G12·C19 in **6**, and nucleoside U21 with C21, in order to stabilise the duplex region. The scissile phosphodiester bond is located within the bulge, except for oligonucleotide **14**, in which the scissile bond is within the double helical stem.

The secondary structure of compounds **4**–**14** was inspected by minimising the free energy by the RNA MFOLD program.[30–32] For compound **8**, two alternative structures, the Gibbs free energies of which differed only by 0.1 kcal mol^{-1} (−12.7 kcal mol^{-1} for **8A**; −12.6 kcal mol^{-1} for **8B**), were obtained. All the other compounds had only one clearly favoured structure according to the MFOLD calculations.

The melting temperatures (T_m) for oligonucleotides **4**–**14** were determined under two different conditions: at pH 7.5 (0.1 M HEPES, $I = 0.1$ M) and at pH 8.5 (0.1 M CHES, $I = 0.1$ M). These buffers were used in the HO^- and Zn^{2+} chelate-catalysed cleavage experiments. The T_m values of **4**–**9** varied from 63 to 67 °C. In all these cases the melting temperatures obtained at pH 7.5 and 8.5 differed by less than 2 °C. The T_m values of **10**–**14** all exceeded 85 °C. The values could not be obtained at a higher accuracy, because the curves did not sufficiently level off to a constant value within the temperature range that could be employed ($T < 100$ °C). The T_m values were concentration independent, consistent with intramolecular duplex formation. The T_m values of a fully 2′-*O*-methylated analogue of **6**, both in the presence of Zn^{2+} ions at pH 6.5 and in the presence of Zn^{2+} chelate at pH = 7.5, were higher than those in the absence of metal ions, suggesting that the metal ions stabilised the hairpin structure. Evidently, under the conditions of the kinetic experiments the oligonucleotides exist in the hairpin forms depicted in Fig. 1.

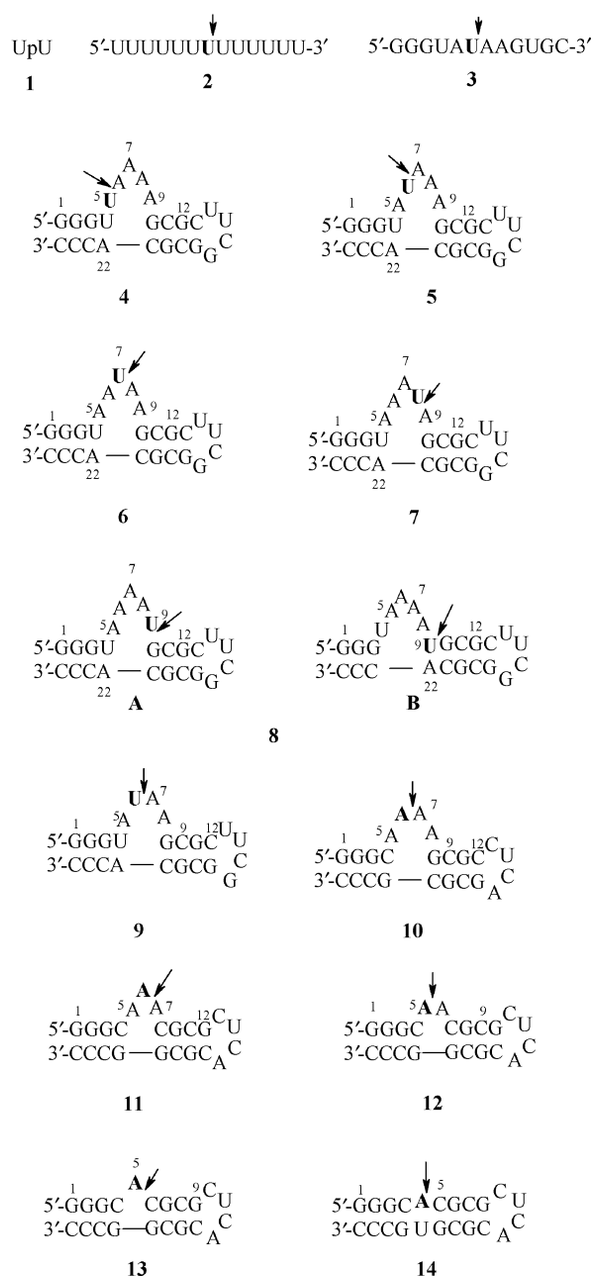

Fig. 1 The structures of the compounds studied. Bold letters refer to ribonucleosides, the other nucleosides being 2′-*O*-methylated. The position of the scissile phosphodiester bond is indicated by an arrow.

The cleavage experiments

The experiments aimed at clarifying the inherent reactivity of compounds **1**, **2** and **4**–**14** were carried out in 0.1 M CHES buffer, at pH 8.4. The predominant reaction under these conditions is the HO^--catalysed cleavage of the phosphodiester bonds;[33,34] this is not accompanied by isomerization of the 3′,5′-phosphodiester bonds to 2′,5′-bonds. The metal ion-promoted cleavage of compounds **3**–**14** was studied under two different conditions: in 10 mM aqueous $Zn(NO_3)_2$ at pH 6.4 and in 5 mM aqueous Zn[12]aneN_3 at pH 7.4. All reactions were carried out at 35 °C, the ionic strength being adjusted to 0.1 M with $NaNO_3$. The composition of aliquots withdrawn at appropriate intervals was analysed by capillary zone electro-

Table 1 Pseudo first-order rate constants of the cleavage of compounds **1**–**14** in CHES buffer and in the presence of Zn^{2+} and Zn^{2+}[12]aneN$_3$ at 35 °C (I = 0.1 M with $NaNO_3$)

Compound	$10^7\ k$(CHES)/s^{-1} [a]	$10^6\ k$(Zn^{2+}[12]-aneN$_3$)/s^{-1} [b]	$10^7\ k$(Zn^{2+})/s^{-1} [c]
1	2.2 ± 0.08	—	—
2	0.9 ± 0.06	—	—
3	—	4.2 ± 0.1	13.0 ± 2.0
4	0.2	4.7 ± 0.3	6.7 ± 0.4
5	2.2 ± 0.1	7.6 ± 0.6	9.0 ± 0.7
6	2.4 ± 0.2	12.5 ± 0.6	24.7 ± 1.9
7	3.2 ± 0.2	9.9 ± 0.4	9.4 ± 0.5
8	0.2	2.2 ± 0.1	3.9 ± 0.2
9	0.9 ± 0.1	5.4 ± 0.2	8.5 ± 0.5
10	[d]	10.3 ± 0.8	15.8 ± 0.8
11	<0.2 [e]	4.5 ± 0.2	14 ± 0.08
12	<0.2 [e]	3.3 ± 0.7	2.3 ± 0.1
13	<0.2 [e]	2.0 ± 0.1	4.0 ± 0.4
14	<0.2 [e]	<0.2 [e]	<0.2 [e]

[a] In 0.1 M CHES, pH 8.4. [b] In 5 mM Zn[12]aneN$_3$ at pH 7.4 adjusted with HEPES buffer. [c] In 10 mM $Zn(NO_3)_2$ at pH 6.4 adjusted with HEPES buffer. [d] Could not be determined, because substrate and products had same migration times in CZE. [e] No reaction after three months.

phoresis (CZE). The formation of two products is initially observed as described in more detail in the Materials and Methods section, showing that during the CZE analysis the 5′-terminal and 3′-terminal fragments are dissociated from each other. It is not, however, possible to tell whether the dissociation takes place as a result of the cleavage or only under the conditions of the CZE analysis. The pseudo first-order rate constants were calculated for the disappearance of the starting material. The observed rate constants for the cleavage of molecules **1**–**14** are listed in Table 1.

Molecular dynamics simulations

To obtain deeper insight into the preferred conformation of the model RNA substrates in view of their inherent reactivity, modelling experiments (simulation of molecular dynamics) were carried out for compounds **4**, **6** and **13**. For comparison, an RNA structure containing only natural ribose residues with the sequence of compound **6**, *i.e.* resembling the five-nucleotide bulge loop domain of the Group I intron from *Tetrahymena thermophila*, was also simulated, since for such a structure NMR data are available.[29]

Among the three modified oligonucleotides, **6** and **13** represent the hydrolytically least and most stable structures, respectively, whereas **4** is an analogue of **6** that differs only in respect of the position of the scissile bond within the bulge. The structures were generated *de novo*, since no experimental initial coordinates were available, and calculated *in aqua* during 1 nanosecond using the AMBER 4.1 force field.[35] The average conformations of these three compounds over the last 100 ps simulations are shown in Fig. 2a–c.

The conformations of the bulge regions of the simulated models were analysed by calculating their backbone torsion angles, sugar puckering and the base-stacking interactions between neighbouring bases. Backbone torsion angles: α, β, γ, δ, ε and ζ, as well as the torsion of the glycosidic bond, were calculated for the trajectories obtained (program CURVES 5.1[36] was used). The notations of the backbone torsion angles are shown in Fig. 3. Table 2 records the average backbone torsion angle values for G3–C11 of **4** and **6**, and for G3–G7 of **13** during the last 100 ps simulation, and the average values of the canonical A-RNA.[37] The glycosidic bonds within the bulges and stem of **4**, **6** and **13** were observed to be in an *anti* conformation. Parameters of similar values (data not shown) were obtained for the reference model containing all-ribo sugar residues.

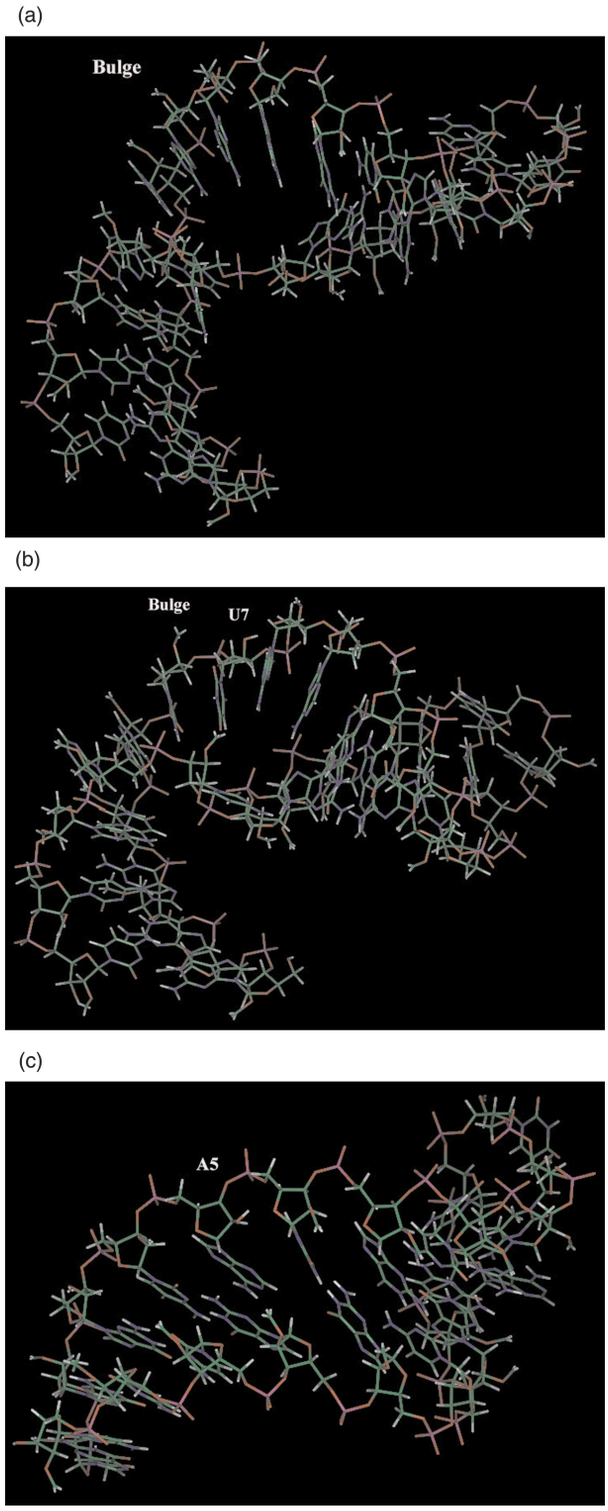

Fig. 2 The average conformations of compound **4** (a), compound **6** (b), and compound **13** (c) during the last 100 ps molecular dynamics simulation.

The sugar-ring puckering was measured by the pseudo-rotation phase angle.[38] Within the bulge region, the 2′-*O*-methylribose conformations fall invariably in the C3′-*endo* range, which is typical for A-RNA. The base-stacking interactions between neighbouring bases were determined by a method published earlier.[39] According to this method, stacking parameter values close to zero indicate that the bases are aligned in accordance with the canonical A-RNA conformation. Values around 3–5 Å are observed when nucleobases lose their parallel alignment or stand aside, which results in a loss of stacking interaction in the respective region. The graphs

Table 2 The average backbone torsion angles (°) of the bulged residues and the two flanking residues to each side for compounds **4**, **6** and **13** during the last 100 ps of molecular dynamics simulation (program CURVES 5.1 [36] was used). The average backbone torsion angles of canonical A-RNA [37] are shown for comparison. Standard deviations are shown in brackets

	α	*β*	*γ*	*δ*	*ε*	*ζ*
4						
G3	152 (18)	−174 (11)	59 (9)	73 (6)	−164 (8)	−65 (9)
U4	−72 (10)	173 (8)	−168 (13)	75 (6)	−148 (9)	−56 (10)
U5	138 (15)	175 (9)	64 (7)	75 (5)	178 (8)	−87 (9)
A6	−74 (9)	177 (10)	−172 (11)	77 (6)	−152 (10)	−65 (9)
A7	−72 (9)	171 (10)	59 (9)	74 (6)	−151 (11)	−68 (9)
A8	−74 (9)	174 (9)	63 (8)	73 (6)	−156 (8)	−68 (7)
A9	−71 (10)	176 (8)	60 (8)	72 (6)	−159 (7)	−68 (7)
G10	−69 (10)	170 (9)	63 (9)	77 (6)	−151 (9)	−62 (9)
C11	−70 (12)	174 (9)	64 (9)	74 (6)	−154 (10)	−66 (7)
6						
G3	−72 (9)	−179 (9)	58 (8)	73 (6)	−154 (8)	−69 (7)
U4	−75 (9)	177 (8)	54 (9)	68 (6)	−157 (8)	−66 (6)
A5	−70 (8)	179 (10)	54 (10)	65 (6)	−156 (9)	−71 (7)
A6	130 (18)	−173 (10)	57 (9)	73 (7)	−161 (9)	−62 (9)
U7	−79 (9)	−180 (8)	−157 (13)	74 (7)	−173 (7)	−82 (8)
A8	−73 (10)	179 (8)	58 (8)	73 (6)	−154 (10)	−67 (8)
A9	−70 (10)	174 (7)	59 (8)	76 (6)	−148 (8)	−63 (8)
G10	−69 (19)	170 (9)	60 (7)	78 (6)	−145 (9)	−64 (8)
C11	−72 (9)	174 (9)	59 (7)	77 (6)	−154 (16)	−66 (9)
13						
G3	−70 (9)	174 (8)	63 (8)	74 (6)	−156 (8)	−66 (8)
C4	−71 (10)	166 (7)	63 (7)	75 (5)	−176 (9)	−66 (8)
A5	−76 (9)	164 (10)	69 (9)	79 (7)	−176 (8)	−89 (9)
C6	−70 (8)	175 (8)	72 (10)	76 (6)	−161 (8)	−66 (8)
G7	−70 (9)	173 (9)	64 (8)	73 (6)	−148 (9)	−66 (9)
A-RNA	−68	178	54	82	−153	−71

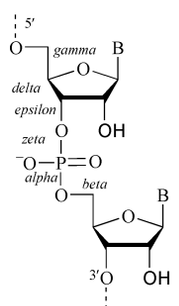

Fig. 3 Backbone torsion angle notations.

showing the changes in pseudorotation angle and stacking parameters undergone during the molecular dynamics simulations are given as supplementary information (ESI).

For substrates **4**, **6** and **13**, conformations within the close vicinity of the scissile phosphodiester bonds were examined in more detail. In all cases, angle 2′O–P–5′O over the entire molecular dynamics simulation remains close to 60°. The conformation of the respective sugar moieties, *viz.* U5 of **4**, U7 of **6** and A5 of **13**, is C3′-*endo*. With all three structures, the cleaving P–5′O bond is oriented parallel to the average plane of the 5′-fragment sugar ring. The distance between the nucleophilic 2′-oxygen and electrophilic phosphorus atoms was observed to vary from 3.6 Å (**6** and **13**) to 4.0 Å (**4**). With **4** and **6**, the attack distance remained constant over the entire simulation, while with **13** it was shortened from the value of 3.8 Å, observed during the first 600 ps, to 3.6 Å during the last 400 ps. The conformation of the phosphodiester bond opposite the bulge also seems to be affected by the structure. The 2′O–P–5′O angles of the phosphodiester bond between C21 and A22 in **4** and in **6** are 118 and 126°, respectively, whereas the corresponding angle in **13** (phosphodiester bond between G17 and G18) is smaller, only 76°. The distance between the 2′-OH nucleophile and the phosphate group varies between 4.0 and 4.2 Å.

Finally, the solvent accessibility of the 2′-hydroxy group of **4**, **6** and **13** was evaluated. With **13**, containing a one-nucleotide bulge, the hydroxy group appears to be buried in a small cavity surrounded by the backbone atoms of the neighbouring residues. Nevertheless, the hydroxy group is well hydrated, water hydrogen bonds being formed (1.1 on the average per simulation frame) by the 2′-oxygen atom as acceptor. The 2′-hydroxy group does not exhibit any tendency to act as donor to neighbouring water molecules. With **4** and **6**, containing a large bulge, the 2′-hydroxy group is present on the solvent-accessible surface and rather well hydrated, although in the case of **4** in only 80% of the frames. Interestingly, the 2′-hydroxy hydrogen of **4** partially compensates this deficiency in hydration by forming weak hydrogen bonds (2.5 Å) to water molecules in nearly 10% of the frames, *i.e.* more frequently than the other two models. Neighbouring 2′-*O*-methyl groups increase the hydrophobic character [40] of the uridine residue vicinity.

Discussion

Conformation of the bulge loop

The results of molecular modelling indicate that the structures of molecules **4**, **6** and **13** are rather similar (Fig. 2a–c) and are also consistent with the unmodified reference model. The structural parameters, such as sugar-ring puckering, base stacking and sugar–phosphate backbone conformation, closely resemble those of A-form RNA.[37]

The backbone torsion angles of both the one- (**13**) and five-nucleotide bulge (**4** and **6**) structures are quite similar to the typical values of A-RNA. Only the *α* value of U5 (138°) and the *γ* value of A6 (−172°) within the 5′-UAAAA-3′ bulge loop (**4**), and the *α* value of A6 (130°) and the *γ* value of U7 (−157°) within the 5′-AAUAA-3′ bulge loop (**6**), are exceptional. In all three cases studied, the bulge appears to be stacked into the structure, rather than being looped out of it. Similar results

have also been obtained by NMR spectroscopy for a one-nucleotide adenosine bulge.[41,42] A looped-out conformation has, in turn, been suggested on the basis of an X-ray structure,[43–46] but this may result from the fact that while NMR experiments and theoretical calculations refer to a situation in solution, X-ray crystallography studies molecules in their solid state.

The disturbance caused by the bulges in the overall duplex structure is surprisingly small. All the sugar rings within the molecules appear to exist in a C3′-*endo*-conformation typical for A-form RNA. Only the A6 and U7 nucleosides of **6** showed some tendency to adopt a C2′-*endo*-puckering. Even in these cases, the C3′-*endo*-conformation clearly predominates. A change to a C2′-*endo*-conformation of bulged and flanking nucleotides in native RNA has previously been reported in the literature, even in the case of one-nucleotide bulges.[41] Similarly, an NMR analysis of the domain of a Group I intron,[29] the parent compound of **6**, shows that nucleoside residues within a 5′-AAUAA-3′ bulge exist as an equilibrium mixture of the two conformers. A possible explanation for this dissimilarity in behaviour is that 2′-*O*-methylribonucleoside units are known to be conformationally more rigid than unsubstituted ribonucleosides,[27,47,48] which is reflected in their resistance to undergo the C2′-*endo* switch. It is also worth noting that the base sequence of **6** is not exactly the same as in the Group I intron, and the flanking sequences are different.

The base moieties adopt an *anti*-conformation, both within the bulges and the double helix. The bases are generally rather well stacked, even at the stem–bulge junction. With **4**, the stacking parameter values indicate marked stacking between the bases A6 and A7, A8 and A9, and at both the 5′- and 3′-stem–bulge junctions. Stacking between the bases U5 and A6 is initially observed, but it is lost after 600 ps. An opposite change in stacking interactions is observed between the bases A7 and A8: the stacking is enhanced after 600 ps. In other words, the stacking pattern is initially disrupted between A7 and A8, but as the simulation proceeds, the discontinuity moves along the molecule. This may be an indication of the molecule existing as an equilibrium mixture of two different conformers. In one of them, bases from U5 to A7, as well as A8 and A9, are well stacked, but the stacking is weaker or non-existent between A7 and A8. In the other form, bases from A6 to A9 are well stacked, and the stacking is lost between U5 and A6. The five-nucleotide bulge of **6** appears to be somewhat more flexible than that of **4**. Efficient stacking occurs between A6 and U7, A8 and A9, and at the 3′-stem–bulge junction, but stacking elsewhere within the bulge is only moderate. Consistent with this observation, the NMR analysis of the Group I intron[29] has suggested the bulge region to be rather dynamic. With **13**, the single bulged nucleoside, adenosine, is well stacked, with the flanking cytosine at the 5′-side, but some discontinuity in the stacking pattern on the 3′-side of the bulge may be observed.

Finally, it is worth bearing in mind that with all the oligonucleotide structures modelled, the geometry in the vicinity of the scissile phosphodiester bond is rather unfavourable for the attack of the 2′-oxygen on the neighbouring phosphodiester group: the angle 2′O–P–5′O is approximately 60°, and hence considerable conformational changes are needed to obtain the co-linear orientation that would allow an in-line displacement of the 5′-linked nucleoside. The distance between the 2′-oxygen and phosphorus atoms is also rather constant, ranging from 3.6 (**6** and **13**) to 4.0 Å (**4**). In each case the 2′-hydroxy group is also rather accessible to solvent, the 2′-oxygen atom being hydrogen-bonded to a water molecule.

The effect of the structure on the inherent reactivity of phosphodiester bonds

Although the results of molecular modelling suggest that the global structures of oligonucleotides **4**, **6**, and to a lesser extent, **13** and their conformational flexibility at the bulge site are rather similar, their susceptibility to hydroxide ion-catalysed cleavage is different. The kinetic data in Table 1 show that the molecular environment within the bulge has a clear influence on the inherent reactivity of the phosphodiester. Similarly to the results previously obtained with hairpin loops,[17] the phosphodiester bonds closer to the double helical stem are clearly less reactive than those in the middle of a bulge. Oligomers **5**–**7**, having a five-nucleotide bulge and the scissile bond in one of the three central positions within the bulge, are cleaved in CHES buffer at pH 8.4 approximately as readily as the linear reference compounds, **1** and **2**. When the scissile phosphodiester bond is moved next to the double helical stem (**4** and **8**), the cleavage rate is decreased by a factor of ten. A phosphodiester bond in the middle of a four-nucleotide bulge loop, as in **9**, is cleaved two to three times less readily than that in a five-nucleotide bulge. As the size of the bulge is still decreased, the cleavage is even more markedly retarded: the phosphodiester bond within three- (**11**), two- (**12**) or one-nucleotide (**13**) bulges, are even more stable than those at the bulge–stem junction of a five-nucleotide bulge (as in **4** or **8**). This is also the case with phosphodiester bonds within the double helical stem (**14**). With structures **11**–**14**, no reaction could be observed in three months. In contrast to the situation with apical hairpin loops,[17] none of the bulge structures turned out to accelerate the phosphodiester cleavage beyond the reactivity of the linear reference molecule.

The intramolecular transesterification reaction is initiated by the attack of the 2′-hydroxy group on the phosphate group, which results in the formation of a pentacoordinated phosphorane species.[49] According to the rules proposed by Westheimer in the 1960's,[50] the entering nucleophile and the departing leaving group both have to occupy an apical position in the transition state of the respective reaction step. The most efficient cleavage may be expected when the angle between the developing and cleaving P–O bonds in the transition state or intermediate is close to 180°. If this favourable in-line conformation cannot be obtained, the reaction takes place *via* the adjacent mechanism,[50] which may involve a rate-limiting pseudorotation.

The molecular modelling results show that none of the molecules **4**, **6** or **13** initially tend to appear in an in-line conformation, but the 2′O–P–5′O angles are of the order of 60°. Yet the reactivity of the phosphodiester bonds seems to be different. The attack distance of the 2′-oxygen nucleophile does not seem to be favourable either. The distances of 3.6 Å (**6** and **13**) and 4.0 Å (**4**), are significantly longer than 3.25 Å, generally regarded as a sufficiently short distance to result in facile attack.[25] The most probable explanation for the apparent inconsistency between the structural information and the kinetic data results is that the calculations refer to the initial state of the reaction, whereas the rate constants are related to the free energy difference between the transition state and the initial state. The fact that the initial conformation deviates significantly from the in-line conformation does not necessarily result in a marked rate-retardation. The crucial factor is how severely the inevitable conformational changes are retarded by the rigidity of the structure. The more flexible the structure is, the easier the conformational rearrangement, and the faster the cleavage of the phosphodiester bond.

Of the three molecules whose structure was studied by molecular modelling, compound **6** is the most reactive. With this compound, only a moderate to good base stacking was observed between the bases within the bulge. In **4** and **13** the stacking patterns were more continuous. Strong base stacking may be taken as an indication of a rigid RNA sequence; either it is the actual reason for, or a consequence of, the rigidity of the strand. Anyway, the discontinuous stacking of **6** reflects the flexibility of the bulge. The other interesting feature of **6** is the tendency of A6 and U7 to adopt a C2′-*endo*-conformation. While with **4** and **13**, the nucleosides around the scissile

phosphodiester bond exist solely in C3′-*endo*-conformation, in **6** a small fraction of a C2′-*endo*-conformation can be observed. We have previously speculated that a C2′-*endo*-conformation might be a prerequisite of the efficient cleavage of a phosphodiester bond, or, alternatively, an indication of structural flexibility.[17] The C2′-*endo*-conformation has also been suggested to favour cleavage in the hammerhead ribozyme reaction.[51]

Based on this, it can be suggested that compound **6** is flexible enough to adopt, without any hindrance, an in-line conformation at the transition state of the cleavage reaction. For this reason, the cleavage is as efficient as that of a linear random coil molecule. Molecules **4** and **13** are more rigid, as indicated by more efficient base stacking and unfavourable sugar ring conformation. Adoption of an in-line conformation becomes, therefore, more difficult, and the reaction is slower.

Soukup and Breaker[16] have previously studied the relationship of phosphodiester conformation and reactivity within various secondary structures. They have determined the in-line fitness (F) of a phosphodiester bond with an equation that takes into account the 2′O–P–5′O angle and the attack distance, and observed that even if the in-line fitness is unfavourable ($F < 0.2$), the reaction rate may still vary within a 500-fold range, approaching that of an unstrained phosphodiester bond of a linear random-coil RNA. The phosphodiester bond, which occupies a favourable in-line conformation ($F = 1$), is, in turn, cleaved only about ten times faster than an unstrained dinucleotide linkage. It appears, therefore, that the initial state conformation does not play a dominant role among the factors affecting the reactivity. This is also consistent with the results obtained in the present work: the F-values[16] obtained for the oligonucleotides **4**, **6** and **13** all range between 0.05 to 0.06.

The situation may well be compared with that of the Pb^{2+}-promoted cleavage of $tRNA^{Phe}$: the X-ray structure suggests the scissile phosphodiester bond does not exist in an in-line conformation, yet the bond is efficiently cleaved in the presence of Pb^{2+} ions.[52] We have also shown previously[17] that the CA phosphodiester bond within the 5′-GCAA-3′ hairpin loop is cleaved at approximately the same rate as within a single-stranded reference compound, in spite of the fact that theoretical calculations using molecular coordinates based on NMR data[53,54] show the structural parameters unfavourable for the cleavage. The 2′O–P–5′O angle of the CA internucleosidic bond appears to be between 71 and 74°, depending on the orientation of the cytidine base, and the attack distance ranges from 3.8 to 4.0 Å.

Metal ion-promoted reactions: cleavage by Zn^{2+}[12]aneN$_3$ and Zn^{2+} aqua ions

Compared to the situation in the absence of metal ion catalysts, and to the cleavage of hairpin loops with metal ions,[18] the bulge structures appear to have an unexpectedly modest influence on the rate of Zn^{2+} or Zn^{2+}[12]aneN$_3$ ion-promoted cleavage. On using Zn^{2+} as a catalyst, the cleavage rates of phosphodiester bonds in different positions within bulges of various size (**4**–**13**) differed by less than one order of magnitude, and with the Zn^{2+} chelate the rate constants varied only within a factor of five. In some cases the reaction rate within the bulge was even higher than that obtained with the random-coil reference compound (**3**). Again the rate constants for the cleavage of the phosphodiester bonds close to the stem (**4**, **8**, **12**, **13**) are smaller than those referring to cleavage in the middle of a bulge (**5**–**7**, **9**, **10**), but the difference is less striking than in the absence of metal ions. The efficiency of the metal ion catalysis compared to that of the hydroxide ion catalysis is increased when the size of the bulge loop is decreased. Molecule **11**, containing a three-nucleotide bulge, seems to be particularly prone to metal ion-dependent cleavage. In fact, the cleavage is as rapid as with the linear reference compound (**3**), while in the absence of Zn^{2+} catalysts the cleavage of **11** is at least one order of magnitude slower than that of the linear reference compounds. Even molecule **13**, having only a one-nucleotide bulge, is quite rapidly cleaved with both Zn^{2+} ion catalysts. Only when the scissile phosphodiester bond is within a double helix is it clearly cleaved less readily than those within bulge loops. For example, with **14** no reaction was observed within three months in the presence of Zn^{2+}[12]aneN$_3$ or Zn^{2+} aqua ion.

A factor that inevitably affects the efficiency of metal ion catalysis is the stability of the metal ion–substrate complex. One may speculate that as the size of the bulge loop decreases, a better metal ion coordination site is formed, and hence the binding of the metal ion catalyst is enhanced. It has been speculated previously, based on an X-ray structure and molecular modelling, that the distance between the adjacent phosphate groups in a bulge structure might be shorter than the average value. A site of higher negative potential would therefore be formed and, as a consequence, metal ion binding be enhanced.[55] Consistent with this, a preferential strand scission by an oligonucleotide conjugate within a bulge has been reported.[23]

As the concentration of the metal-bound substrate molecules increases, the rate of the metal ion-dependent cleavage increases in proportion to the concentration. This concentration-based rate enhancement appears to be significant enough to compensate the loss in the inherent reactivity that results from the rate-retarding effect of the increased rigidity of the sugar–phosphate backbone close to the double helical stem.

Conclusions

The size of the bulge loop and the position of the phosphodiester bond within it have a considerable influence on the inherent reactivity as observed in the case of the hydroxide ion catalysed cleavage of phosphodiester bonds. Clear correlation between the rate of the cleavage and the initial state conformation around the scissile phosphodiester bond cannot be observed. The increasing flexibility of the bulge, however, facilitates the reaction, the central bonds in a five-nucleotide bulge being cleaved as rapidly as linear random-coil RNA. With one- and two-nucleotide bulges the inherent reactivity of the phosphodiester bonds is more than one order of magnitude lower.

The cleavage promoted by Zn^{2+} or its 1,5,9-triazacyclododecane chelate is not as susceptible to the size of the bulge and the position of the scissile bond within it. The cleavage rate at a one-nucleotide bulge, for example, is still about 20% of that at the central bonds of a five-nucleotide bulge. Accordingly, on developing artificial cleaving agents based on metal ions, even a small bulge formed upon hybridisation of the cleaving agent with the target appears to allow reasonably fast chain cleavage, in striking contrast to a fully double helical structure. Possibly a small bulge offers a good metal ion coordination site. Even though the inherent reactivity of phosphodiester bonds within small bulges may be reduced due to structural reasons, more efficient binding compensates the reactivity loss.

Materials and methods

Materials

The chimeric ribo/2′-*O*-methylribooligonucleotides (**2**–**14**) were synthesised from commercial 2′-*O*-methylated (Glenn Research) and 2′-*O*-[1-(2–fluorophenyl)-4-methoxypiperidin-4-yl] (2′-*O*-Fpmp) protected (Cruachem) building blocks by a conventional phosphoramidite strategy, according to the standard RNA-coupling protocol of ABI 392 DNA/RNA Synthesizer. The protecting groups were removed and the crude oligonucleotides were purified as described previously.[18]

3′,5′-UpU (**1**) was a product of Sigma, and it was used as received. 1,5,9-Triazacyclododecane was a product of Aldrich, and it was used as received to prepare the Zn^{2+}[12]aneN$_3$ chelate. All the other reagents were of reagent grade. All the buffer solutions were prepared in sterilised water, and sterilised equipment was used for handling the solutions.

Melting temperature measurements of the oligonucleotides

The melting curves were recorded on a Perkin-Elmer Lambda 2 UV spectrometer equipped with a PTP-6 temperature programmer that consisted of two electronic control units and Peltier cell housing blocks. The temperature was increased at a rate of 1 °C min^{-1} over the temperature range 15–90 °C. The change of UV absorption was followed at 260 nm in 0.1 M HEPES buffer [*N*-(2-hydroxyethyl)piperazine-*N*′-ethanesulfonic acid, $pK_a = 7.5$ at 25 °C] at pH 7.5 ($I = 0.1$ M with $NaNO_3$) and in 0.1 M CHES buffer (cyclohexylaminoethanesulfonic acid, $pK_a = 9.5$ at 25 °C) at pH = 8.5 ($I = 0.1$ M with $NaNO_3$). The melting temperatures for oligonucleotides **10**–**14** could not be determined, since, owing to their high melting temperature, the curves did not sufficiently level off to a constant value in the temperature range that could be employed.

Kinetic measurements

The reactions were carried out in Eppendorf tubes immersed in a water bath, the temperature of which was maintained at 35 ± 0.1 °C. The pH of the reaction solutions was adjusted by using CHES and HEPES buffers. The metal ions were introduced as nitrates, and the ionic strength was adjusted with sodium nitrate. The pH was checked after the addition of metal ions, and adjusted when necessary. The total volume of the oligonucleotide reaction solutions ranged from 400 to 440 μL, and it contained 2 OD units of the oligonucleotide. *p*-Toluenesulfonate ion was used as an internal standard. Its concentration was adjusted to give a peak of similar size to that of the substrate at the beginning of the reaction.

Aliquots (20 μL) withdrawn at suitable intervals were immediately cooled to 0 °C. The Zn^{2+}[12]aneN$_3$ promoted reaction (pH 7.4) was quenched by adding aqueous HCl (1.0 μL of 1.0 M solution). The samples were kept in the freezer until analysed.

The analysis of samples

The aliquots of UpU reactions were analysed by RP-HPLC using a Hypersil RP-18 column (250 × 4 mm, 5 μm particle size). The chromatographic conditions were: [flow rate 1 mL min^{-1}, eluent A acetic acid buffer (0.1 M pH 4.3) containing 0.1 M NH_4Cl, and eluent B the same buffer containing 5% acetonitrile] 0–8 min eluent A and 8–20 min eluent B. The retention time of UpU was 14 min. Detection at 260 nm was employed.

Aliquots of the oligonucleotide reactions were analysed by capillary zone electrophoresis (CZE). CZE analysis was performed on a Hewlett Packard ^{3D}CE equipment. A fused silica capillary (75 μm id, 112.5 cm total length, 104 cm effective length) was employed. The samples were analysed using 0.1 M phosphate buffer pH 2.7 and inverted polarity. The voltage applied was −30 kV. The temperature of the capillary was kept at 25 °C. The samples were injected using hydrodynamic injection with 50 mbar for 10 s. Between each analytical run the capillary was flushed first with water for 2 min, then for 3 min with 10 mM aqueous HCl and finally for 3 min with the background electrolyte. The oligonucleotides and the internal standard were analysed by UV detection at 260 and 220 nm, respectively. 1.0 μL of aqueous acetic acid (HOAc–H_2O 1 : 3, *v*/*v*) was added to the samples withdrawn from the CHES buffer solutions to adjust the pH close to that of the background electrolyte buffer.

Using the analysis conditions described above, the migration times of oligonucleotides (**2**–**14**) ranged from 18 to 23 min. The migration time of the internal standard was 15 minutes. The migration times of the substrates and products depended on the chain length, base composition and also the buffer employed in the reaction solution. The initial cleavage products, *viz.* the 5′-fragment bearing a terminal 2′,3′-cyclic monophosphate group[56] and released 3′-fragment, appeared as separate peaks. The separation of oligonucleotide 2′- and 3′-phosphates formed upon hydrolysis of the initial product bearing the 2′,3′-cyclic phosphate group could not be observed under the given conditions. In CHES buffers, partial dephosphorylation of the 2′/3′-phosphates to the 3′-OH free oligomer was observed.

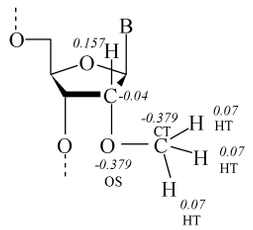

Fig. 4 Force field parameters for the 2′-*O*-methylribosyl moiety.

Calculation of rate constants

The pseudo first-order rate constants for the cleavage of the starting material into two fragments were calculated by applying the integrated first-order rate law to the disappearance of the starting material. The peak area was first normalised by dividing the area observed by the migration time. The normalised area of the starting material was then divided by the normalised area of the internal standard. However, in the case of the Zn^{2+}-promoted and base catalysed cleavage of **8**, the cleavage product bearing the terminal 2′,3′-cyclic phosphate group had the same migration time as the starting material. In these cases the rate constants were calculated by applying the integrated first-order rate law to the appearance of the released 3′-terminal fragment.

Molecular modelling

The model molecules (sequences as those of compounds **4**, **6** and **13** plus an unmodified analogue of **6**) were built using the BIOPOLYMER module of the INSIGHTII[57] suite of programs. Their geometry was optimised by a short *in vacuo* energy minimisation performed using the Discover module (AMBER force field, 500 steps of Steepest Descent algorithm, then 500 steps of Conjugate Gradients). The force field parameters for the 2′-*O*-methylribosyl moiety were developed using the GAUSSIAN94[58] and RESP[59] programs. This led to assigning the parameters shown in Fig. 4 to the modified area.

The same models were then built in the AMBER 4.1[60] suite of programs using the model building modules (PREP, LINK, EDIT, PARM). The RNA model molecules had added sodium counterions near their phosphate centres and each of them was solvated in a rectangular periodic boundary conditions (PBC) box (a 10 Å thick water layer was maintained in all dimensions around the RNA molecules). The total number of water molecules ranged from 3223 to 3836, depending on the size of the model. The initial coordinates for the simulations were taken from the Discover geometry optimisations (see above). The simulations were carried out using the Sander module from AMBER 4.1 run on a CRAY J-916 machine in the Poznan Supercomputing and Networking Centre. The 1995 version of the AMBER forcefield[35] was used. The protocol for the simulations followed the procedure applied by Cheatham and Kollman[61] and consisted of an equilibration procedure (alternating energy minimisation and short molecular dynamics runs with gradually relieved constraints on the DNA molecule) and 1 ns of unrestrained molecular dynamics in 300 K with the long-range electrostatic interactions treated using the particle-mesh Ewald summation method.[62] The resultant trajectories were analysed and visualised on an Iris Indigo^2 workstation using the INSIGHTII software (ANALYSIS module), the

CURVES 5.1 program[36] and our own procedures, especially in regard to the analysis of base stacking stability.[39]

Acknowledgements

Financial support from the Academy of Finland (H. L.) and access to the resources of the Poznan Supercomputer and Networking Centre (R. A.) is gratefully acknowledged.

References

1 B. N. Trawick, A. Daniher and J. K. Bashkin, *Chem. Rev.*, 1998, **98**, 939.
2 J. K. Bashkin, U. Sampath and E. Frolova, *Appl. Biochem. Biotechnol.*, 1995, **54**, 43.
3 V. V. Vlasov, V. N. S'ilnikov and M. A. Zenkova, *Mol. Biol.*, 1998, **32**, 50.
4 M. Komiyama, *J. Biochem.*, 1995, **118**, 665.
5 A. De Mesmaeker, R. Häner, P. Martin and H. Moser, *Acc. Chem. Res.*, 1995, **28**, 366.
6 R. Häner, J. Hall, A. Pfitzer and D. Hüsken, *Pure Appl. Chem.*, 1998, **70**, 111.
7 B. F. Baker, S. S. Lot, J. Kringel, S. Cheng-Flournoy, P. Villiet, H. M. Sasmor, A. M. Siwkowski, L. L. Chappel and J. R. Morrow, *Nucleic Acids Res.*, 1999, **27**, 1547.
8 S. Kuusela and H. Lönnberg, *Met. Ions Biol. Syst.*, 1996, **32**, 272.
9 S. Kuusela and H. Lönnberg, *Curr. Top. Solution Chem.*, 1997, **2**, 29.
10 J. R. Morrow, *Met. Ions Biol. Syst.*, 1996, **33**, 561.
11 D. M. Perreault and E. V. Anslyn, *Angew. Chem., Int. Ed. Engl.*, 1997, **36**, 432.
12 K. P. McCue and J. R. Morrow, *Inorg. Chem.*, 1999, **38**, 6136.
13 D. M. Epstein, L. L. Chappell, H. Khalili, R. M. Supkowski, W. DeW. Horrocks Jr. and J. R. Morrow, *Inorg. Chem.*, 2000, **39**, 2130.
14 Z. Wieczorek, E. Darzynkiewicz, S. Kuusela and H. Lönnberg, *Nucleosides Nucleotides*, 1999, **18(1)**, 11.
15 D. A. Usher and A. H. McHale, *Proc. Natl. Acad. Sci. U.S.A.*, 1976, **73**, 1149.
16 G. Soukup and R. Breaker, *RNA*, 1999, **5**, 1308.
17 I. Zágorowska, S. Mikkola and H. Lönnberg, *Helv. Chim. Acta*, 1999, **82**, 2105.
18 I. Zágorowska, S. Mikkola and H. Lönnberg, *Nucleic Acids Res.*, 1998, **26**, 3392.
19 S. Kuusela, A. Azhayev, A. Guzaev and H. Lönnberg, *J. Chem. Soc., Perkin Trans. 2*, 1995, 1197.
20 S. Kuusela, A. Guzaev and H. Lönnberg, *J. Chem. Soc., Perkin Trans. 2*, 1996, 1895.
21 For a review on metal ion-promoted cleavage of different RNA motifs, see T. Pan, D. M. Long and O. C. Uhlenbeck, in *The RNA World*, Cold Spring Harbor Laboratory Press, Plainview, NY, 1993, p. 271.
22 K. A. Kolasa, J. R. Morrow and A. P. Sharma, *Inorg. Chem.*, 1993, **32**, 3983.
23 J. Hall, D. Hüsken and R. Häner, *Nucleic Acids Res.*, 1996, **24**, 3522.
24 D. Hüsken, G. Goodall, M. J. J. Blommers, J. Jahnke, R. Häner and H. E. Moser, *Biochemistry*, 1996, **35**, 16591.
25 R. A. Torres and T. C. Bruice, *Proc. Natl. Acad. Sci. U.S.A.*, 1998, **95**, 11077.
26 T. M. Woolf, *Antisense Res. Dev.*, 1995, **5**, 227.
27 M. Popenda, E. Biala, J. Mielecki and R. W. Adamiak, *Nucleic Acids Res.*, 1997, **25**, 4589.
28 V. A. Bloomfield, D. M. Crothers and I. Tinoco Jr, *Nucleic Acids, Structures, Properties and Functions*, University Science Books, Sausalito, CA, U.S.A, 2000.
29 K. J. Luebke, S. M. Landry and I. Tinoco Jr., *Biochemistry*, 1997, **36**, 10246.
30 M. Zuker, D. H. Mathews and D. H. Turner, in *RNA Biochemistry and Biotechnology*, ed. J. Barciszewski and B. F. C. Clark, NATO ASI Series, Kluwer Academic Publisher, the Netherlands, 1999, p. 11.
31 D. H. Mathews, J. Sabina, M. Zuker and D. H. Turner, *J. Mol. Biol.*, 1999, **288**, 911.
32 MFOLD program is available on the website: http://www.bioinfo.math.rpi.edu/~zukerm/rna/
33 P. Järvinen, M. Oivanen and H. Lönnberg, *J. Org. Chem.*, 1991, **56**, 5396.
34 S. Kuusela and H. Lönnberg, *J. Chem. Soc., Perkin Trans. 2*, 1994, 2109.
35 W. D. Cornell, P. Cieplak, C. I. Bayly, I. R. Gould Jr., K. M. Merz, D. M. Ferguson, D. C. Spellmeyer, T. Fox, J. W. Caldwell and P. A. Kollman, *J. Am. Chem. Soc.*, 1995, **117**, 5179.
36 R. Lavery and H. Sklenar, *J. Biomol. Struct. Dyn.*, 1998, **6**, 63.
37 W. Saenger, *The Structure of Nucleic Acids*, Springer, Berlin, 1984.
38 H. P. M. De Leeuw, C. A. G. Haasnoot and C. Altona, *Isr. J. Chem.*, 1980, **20**, 108.
39 L. Bielecki, T. Kulinski and R. Adamiak, in *RNA Biochemistry and Biotechnology*, ed. J. Barciszewski and B. F. C. Clark, NATO ASI Series, Kluwer Academic Publisher, the Netherlands, 1999, p. 73.
40 D. A. Adamiak, J. Milecki, M. Popenda, R. W. Adamiak, Z. Dauter and W. R. Rypniewski, *Nucleic Acids Res.*, 1997, **25**, 4599.
41 V. Thiviyanathan, A. B. Guliaev, N. B. Leontis and D. G. Gorenstein, *J. Mol. Biol.*, 2000, **300**, 1143.
42 P. N. Borer, Y. Lin, S. Wang, M. W. Roggenbuck, J. M. Gott, O. C. Uhlenbeck and I. Pelczer, *Biochemistry*, 1995, **34**, 6488.
43 C. Sudarsanakumar, Y. Xiong and M. Sundaralingam, *J. Mol. Biol.*, 2000, **299**, 103.
44 J. R. Cate, A. R. Gooding, E. Podell, K. Thou, B. L. Golden, C. E. Kundrot, T. Cech and J. A. Doudna, *Science*, 1996, **273**, 1678.
45 K. Valegård, J. B. Murray, P. G. Stockley, N. J. Stonehouse and L. Liljas, *Nature*, 1994, **371**, 623.
46 E. Ennifar, M. Yusupov, P. Walter, R. Marquet, B. Ehresmann, C. Ehresmann and P. Dumas, *Structure*, 1999, **7**, 1439.
47 S. Uesugi, H. Miki, M. Ikehara, H. Iwahashi and Y. Kyogoku, *Tetrahedron Lett.*, 1979, **42**, 4073.
48 W. Guschlbauer and K. Jankowski, *Nucleic Acids Res.*, 1980, **8**, 1421.
49 M. Oivanen, S. Kuusela and H. Lönnberg, *Chem. Rev.*, 1998, **98**, 961.
50 F. H. Westheimer, *Acc. Chem. Res.*, 1968, **1**, 70.
51 R. A. Torres and T. C. Bruice, *J. Am. Chem. Soc.*, 2000, **122**, 781.
52 R. S. Brown, B. F. Hingerty, J. C. Dewan and A. Klug, *Nature*, 1983, **303**, 543.
53 F. M. Jucker, H. A. Heus, P. F. Yip, E. H. M. Moors and A. Pardi, *J. Mol. Biol.*, 1996, **204**, 968.
54 F. M. Jucker, H. A. Heus, P. F. Yip, E. H. M. Moors and A. Pardi, PDB identification code 1ZIH, 1996.
55 S. Portmann, S. Grimm, C. Workman, N. Usman and M. Egli, *Chem. Biol.*, 1996, **3**, 173.
56 S. Kuusela and H. Lönnberg, *J. Chem. Soc., Perkin Trans. 2*, 1994, 2301.
57 *InsightII Version 2.3.0*, *December 1993*, *User Guide, Part I*, Biosym Technologies Inc., San Diego, 1993.
58 *Gaussian 94*, *Revision C.3*, Gaussian Inc., Pittsburgh, 1995.
59 P. Cieplak, W. D. Cornell, C. Bayly and P. Kollman *J. Comput. Chem.*, 1995, **16**, 1357.
60 D. A. Pearlman, D. A. Case, J. Caldewell, W. S. Ross, T. E. Cheatham, D. M. Ferguson, G. L. Seibel, U. C. Sigh, P. Weiner and P. A. Kollman, *Amber Version 4.1*, University of California, 1995.
61 T. E. Cheatham and P. A. Kollman, *J. Am. Chem. Soc.*, 1997, **119**, 4805.
62 U. Essmann, L. Perera, M. L. Berkowitz, T. Darden, H. Lee and L. G. Pedersen, *J. Chem. Phys.*, 1995, **103**, 8577.